Electron-phonon interactions and related physical properties of metals from linear-response theory

S. Y. Savrasov
Max-Planck-Institut für Festkörperforschung, Heisenbergstrasse 1, 70569 Stuttgart, Germany

D. Y. Savrasov
P. N. Lebedev Physical Institute, Leninskii prospekt 53, 117924 Moscow, Russia
(Received 11 April 1996; revised manuscript received 13 September 1996)

Spectral distribution functions of electron-phonon interaction $\alpha^2F(\omega)$ obtained by *ab initio* linear-response calculations are used to describe various superconducting and transport properties in a number of elemental metals such as Al, Cu, Mo, Nb, Pb, Pd, Ta, and V. Their lattice dynamics and self-consistently screened electron-phonon coupling are evaluated within local density functional theory and using a linear-muffin-tin-orbital basis set. We compare our theoretical $\alpha^2F(\omega)$ with those deduced from the tunneling measurements and find a close agreement between them. Temperature-dependent electrical and thermal resistivities as well as transport constants λ_{tr} also agree well with the experimental data. The values of λ_{tr} are close to the electron-phonon coupling parameter λ. For the latter a very good agreement with specific-heat measurements was found without any paramagnon contribution, except in Pd. We conclude that our method provides the description of electron-phonon interactions in tested materials with an accuracy of 10%. [S0163-1829(96)05448-3]

I. INTRODUCTION

Electron-phonon interaction (EPI) in metals is a subject of intensive theoretical and experimental investigations. The interest in this problem arises from a variety of physical phenomena such as electrical and thermal resistivities, renormalization of the electronic specific heat (electronic mass enhancement), and, of course, superconductivity, and for a quantitative understanding of those a proper description of the EPI is required.[1] Moreover, the reliable estimation of the EPI parameters in a particular case of high-temperature superconductivity may be decisive for recognizing the nature of this phenomenon. Unfortunately, even for some transition metals we have controversial experimental and theoretical data related to the estimation of the coupling constant λ. The analysis is complicated by possible parallel processes of spin fluctuations, for example, in the problem[2] of renormalization of specific heat and T_c or proximity effects in the tunneling data.[3] To extract the quantities of interest one has to use some theoretical calculations and models. In this situation fully *ab initio* calculations of the one-electron spectra and phonon dispersions based on density functional theory[4] (DFT) are most preferable. Applicability of the popular local density approximation[5] (LDA) for the functional and treatment of the one-electron band structures as spectra of low-energy electronic excitations were checked many times and there exist a large theoretical and experimental experience.[6] This allows us to conclude that even having been formally ground-state theory, DFT is a good starting point for investigating the electron-phonon interaction.

Many previous attempts to compute EPI, in particular, for transition metals, have focused on calculating merely the electronic contribution to this quantity,[7] while the phonon frequencies $\omega_{\mathbf{q}\nu}$ and the eigenvectors $\eta_{\mathbf{q}\nu}$ were usually taken from inelastic neutron-scattering data. There, the self-consistent adjustment of the one-electron potential to the phonon distortion was replaced by either a rigid-ion approximation[8] (RIA) or the most popular rigid-muffin-tin approximation[9] (RMTA). For isotropic metals, having a large density of states at the Fermi energy, the RMTA works well in many cases, since the efficient electronic screening limits the change of the potential in the immediate vicinity of the displaced atom. However, there are some known problems of the RMTA in transition metals. For example, anisotropy of the mass enhancement factor was not reproduced by the RMTA in Nb.[10]

Accurate $\omega_{\mathbf{q}\nu}$ and $\eta_{\mathbf{q}\nu}$ as well as self-consistently screened electron-phonon interaction can be calculated within the total-energy frozen-phonon approach using the supercells.[11–14] However, there is a serious drawback of this method. A sufficiently large number of phonon wave vectors $\mathbf{q}$ must be sampled in the Brillouin zone to get a good estimate of the average coupling strength λ. A separate frozen-phonon calculation is required for each $\mathbf{q}$ and for each studied mode. For small phonon wave vectors this requires very large supercells. With the crude sampling allowed by the limited size of the supercell, the accuracy of $\mathbf{q}$ integrated quantities like λ is usually low.

Another technique which can be employed for calculating the self-consistent change in the potential is the perturbative approach[11] applicable for any $\mathbf{q}$. The key quantity of this method is an independent-particle polarizability function. After applying the first-order perturbation theory and expanding the first-order changes in the one-electron wave functions over the basis of unperturbed Bloch states, the polarizability is expressed via the double sum over occupied and unoccupied states. Winter[15] has successfully applied this method to calculate λ in Al. Unfortunately, the perturbative approach has several drawbacks. First, the slowly convergent sum over the excited states requires their preliminary calculation by diagonalizing the unperturbed Hamiltonian matrix of very large dimension. Second, the self-consistency in this

method is done by inverting the dielectric matrix of the crystal which is a relatively time-consuming problem.

To date, the most efficient technique developed to calculate the lattice dynamics is the solid-state generalization[16] of the Sternheimer method.[17] This method is not limited to **q**'s commensurate with the lattice as the frozen-phonon approach and it does not require the knowledge of all unperturbed states as the perturbative approach. In the previous paper[18] (referred hereafter as I) we have given a full description of this approach in the framework of the linear-muffin-tin-orbital (LMTO) method.[19] The latter allows us to facilitate the treatment of localized valence wave functions. In this paper we present details of generalizing this linear-response method to compute the wave-vector-dependent electron-phonon coupling. (A brief report of this work has appeared already[20].) We evaluate the spectral distribution functions $\alpha^2F(\omega)$ of the EPI from the phonon linewidths $\gamma_{\mathbf{q}\nu}$ according to the approach developed by Allen[21] in the superconductivity theory.[22] The electron-phonon matrix elements are calculated in the LMTO representation. Due to incompleteness of the basis sets in band-structure calculations the corrections to these matrix elements are shown to exist and explicitly taken into account. The incomplete-basis-set (IBS) corrections appear here in the same manner as in the calculation of the dynamical matrix within the linear-response theory[18] or when calculating the forces within the total-energy frozen-phonon approach in terms of the LMTO method.[23]

We apply the developed scheme to compute electron-phonon coupling for a large number of elemental metals. We also present calculations of their phonon dispersion curves. The results of computed transport properties such as temperature-dependent phonon-limited electrical resistivities and thermal conductivities obtained as low-order variational solutions of the Boltzman equation are also given. The method of calculating the transport properties is analogous to that used in the supeconductivity theory and is based[24] on calculating the transport spectral functions $\alpha^2_{\mathrm{tr}}F(\omega)$. All the results presented in this paper are completely *ab initio* and no adjustable parameters have been used in the calculations.

The rest of the paper is organized as follows. In Sec. II, we derive the formulas for calculating the electron-phonon matrix elements and briefly review the method of finding superconducting and transport properties. Section III presents the results of the calculations for phonon dispersions, electron-phonon interactions, and related properties for a number of elemental metals such as Al, Cu, Mo, Nb, Pb, Pd, Ta, and V. Section IV concludes the paper.

II. METHOD

The central problem in calculating the electron-phonon interaction is the evaluation of changes in the electronic Hamiltonian caused by atomic displacements. This generally requires the knowledge of the full low-energy excitation spectrum of the metal: the quasiparticle energies and the phonon frequencies. The calculations of vibrational properties are, in principle, within the scope of the density-functional based methods. Finding the quasiparticle excitation spectra is, on the other hand, a much more difficult many-body problem. In the following we always assume that the quasiparticle energies are necessarily approximated by the LDA energy bands.

In the framework of the density-functional linear-response method the problem of calculating the phonon spectra and the electron-phonon interaction is reduced to finding the first-order variations in the one-electron wave functions, the charge density and the effective potential induced by the presence of a phonon with a given wave vector **q.** In paper I we have described an approach for the self-consistent solution of this problem in the framework of the LMTO method. In this paper we test the produced self-consistent change in the one-electron potential as the potential of electrons interacting with the phonon mode $\omega_{\mathbf{q}\nu}$. Our task is to evaluate the electron-phonon matrix element $g^{\mathbf{q}\nu}_{\mathbf{k}+\mathbf{q}j',\mathbf{k}j}$ The latter is conventionally written in the form

$$g^{\mathbf{q}\nu}_{\mathbf{k}+\mathbf{q}j',\mathbf{k}j}=\langle \mathbf{k}+\mathbf{q}j'\,|\,\delta^{\mathbf{q}\nu}V_{\mathrm{eff}}|\mathbf{k}j\rangle, \tag{1}$$

where both states $\psi_{\mathbf{k}j}$ and $\psi_{\mathbf{k}+\mathbf{q}j'}$ have the Fermi energy ϵ_F and where the change in the potential is transformed from the Cartesian system to the system associated with the eigenvectors $\eta_{\mathbf{q}\nu}(R\mu)$ of a particular $\mathbf{q}\nu$ mode:

$$\delta^{\mathbf{q}\nu}V_{\mathrm{eff}}=\sum_{R,\mu}\frac{\eta_{\mathbf{q}\nu}(R\mu)}{(M_R\omega_{\mathbf{q}\nu})^{1/2}}\frac{\delta^+V_{\mathrm{eff}}}{\delta R_\mu}, \tag{2}$$

where M_R are the nuclei masses. Here and in the following the same notations as in I are used.

It is not obvious but the expression (1) for $g^{\mathbf{q}\nu}_{\mathbf{k}+\mathbf{q}j',\mathbf{k}j}$ should be corrected for the incompleteness of the basis functions. To see this we have to repeat the standard quantum-mechanical derivation of the Fermi ''golden rule'' for the wave functions represented in terms of the LMTO basis set. The derivation considers a scattering rate for transitions from an initial unperturbed state into a final perturbed state at the time moment t. For the illustration let us take some Hamiltonian H and a perturbation ΔV. To simplify the notations we denote the initial state as $\psi_s(t)$ and the final state as $\tilde{\psi}_r(t)$. The scattering rate is given by the overlap integral squared:

$$P_{rs}(t)=|\langle\tilde{\psi}_r(t)\,|\,\psi_s(t)\rangle|^2, \tag{3}$$

In the time-dependent formulation we write

$$i\frac{\partial\psi_s(t)}{\partial t}=H\psi_s(t), \tag{4}$$

and

$$i\frac{\partial\tilde{\psi}_r(t)}{\partial t}=(H+\Delta V)\tilde{\psi}_r(t). \tag{5}$$

We now use a variational estimate for the wave fucntions like it is done in the LMTO method

$$\psi_s(t)=\sum_\alpha\chi_\alpha A^s_\alpha(t), \tag{6}$$

Eq. (4) becomes

$$i\sum_\alpha\langle\chi_\beta|\chi_\alpha\rangle\frac{\partial A^s_\alpha(t)}{\partial t}=\sum_\alpha\langle\chi_\beta|H|\chi_\alpha\rangle A^s_\alpha(t) \tag{7}$$

or in the matrix notations

$$i\hat{O}\frac{\partial A^s(t)}{\partial t}=\hat{H}A^s(t), \tag{8}$$

where the overlap matrix $O_{\beta\alpha}=\langle\chi_\beta|\chi_\alpha\rangle$ and the Hamiltonian matrix $H_{\beta\alpha}=\langle\chi_\beta|H|\chi_\alpha\rangle$. Using a standard substitution $A^s(t)=\exp(-i\epsilon_s)A^s$, Eq. (8) transforms to the matrix eigenvalue problem $\hat{H}\ A^s=\epsilon_s\hat{O}A^s$ the solution of which gives the best (in the variational sense) estimate for the eigenfunctions of the operator H at a given basis $\{\chi\}$.

As we have argued in I in order to obtain the best variational estimate for the perturbed wave function $\tilde{\psi}_r(t)$ to the first order, one should take into account both the change in the expansion coefficients, ΔA^r, and the change in the basis set, $\Delta\chi_\alpha$, as seen from varying Eq. (6). Keeping the contributions to linear order, the overlap integral between the initial and final state has the form

$$\langle\tilde{\psi}_r(t)|\psi_s(t)\rangle=\delta_{rs}+\langle A^r(t)|\Delta\hat{O}|A^s(t)\rangle+\langle\Delta A^r(t)|\hat{O}|A^s(t)\rangle, \tag{9}$$

where $\Delta A^r(t)$ can found from the solution of the equation obtained after the linearizing of (5) or varying (7), i.e.,

$$i\Delta\hat{O}\frac{\partial A^r(t)}{\partial t}+i\hat{O}\frac{\partial\Delta A^r(t)}{\partial t}=\Delta\hat{H}A^r(t)+\hat{H}\Delta A^r(t) \tag{10}$$

or, equivalently,

$$i\hat{O}\frac{\partial\Delta A^r(t)}{\partial t}=(\Delta\hat{H}-\epsilon_r\Delta\hat{O})A^r(t)+\hat{H}\Delta A^r(t), \tag{11}$$

where both the change in the Hamiltonian and the overlap matrix contain the terms associated with the variation of the basis functions, i.e.,

$$\Delta O_{\beta\alpha}=\langle\Delta\chi_\beta|\chi_\alpha\rangle+\langle\chi_\beta|\Delta\chi_\alpha\rangle,$$
$$\Delta H_{\beta\alpha}=\langle\chi_\beta|\Delta V|\chi_\alpha\rangle+\langle\Delta\chi_\beta|H|\chi_\alpha\rangle+\langle\chi_\beta|H|\Delta\chi_\alpha\rangle. \tag{12}$$

In order to solve Eq. (11) we use the following representation:

$$\Delta A^r(t)=e^{-i\hat{O}^{-1}\hat{H}t}\Delta B^r(t). \tag{13}$$

Then, the coefficients $\Delta B^r(t)$ are given by

$$\Delta B^r(t)=-i\int_a^t e^{i\hat{O}^{-1}\hat{H}\tau}\hat{O}^{-1}(\Delta\hat{H}-\epsilon_r\Delta\hat{O})A^r(\tau)d\tau, \tag{14}$$

and the matrix element (9) is rewritten as follows:

$$\langle\tilde{\psi}_r(t)|\psi_s(t)\rangle=\delta_{rs}+\langle A^r|\Delta\hat{O}|A^s\rangle e^{i(\epsilon_r-\epsilon_s)t}-i\int_a^t\langle A^r|\Delta\hat{H}-\epsilon_s\Delta\hat{O}|A^s\rangle e^{i(\epsilon_r-\epsilon_s)\tau}d\tau. \tag{15}$$

As a common practice, we assume that the perturbation is switched on adiabatically at the time moment $t=-\infty$. For the scattering rate per unit time we obtain the expression

$$w_{rs}=\lim_{T\to\infty}\frac{1}{T}P_{rs}(T)=2\pi\delta(\epsilon_r-\epsilon_s)\left|\langle A^r|\Delta\hat{H}-\epsilon_r\Delta\hat{O}|A^s\rangle\right|^2. \tag{16}$$

As one can see, this formula differs from the well-known expression for w_{rs} by the presence of the contributions associated with the change in the basis functions as follows from the definitions (12).

We now restore the original notations. The electron-phonon matrix element $\langle A^r|\Delta\hat{H}-\epsilon_r\Delta\hat{O}|A^s\rangle$ must describe the scattering of an electron at the Fermi surface from the state $|\mathbf{k}j\rangle$ to the state $|\mathbf{k}+\mathbf{q}j'\rangle$ via the phonon perturbation $\delta^{\mathbf{q}\nu}V_{\rm eff}$. We therefore set $\{r\}\equiv\{\mathbf{k}+\mathbf{q}j'\}$, $\{s\}\equiv\{\mathbf{k}j\}$, and using the definitions (12), we obtain

$$g^{\mathbf{q}\nu}_{\mathbf{k}+\mathbf{q}j',\mathbf{k}j}=\langle\mathbf{k}+\mathbf{q}j'|\,\delta^{\mathbf{q}\nu}V_{\rm eff}|\mathbf{k}j\rangle+\left\langle\sum_\alpha\ \delta^{\mathbf{q}\nu}\chi_\alpha^{\mathbf{k}-\mathbf{q}}A_\alpha^{\mathbf{k}+\mathbf{q}j'}\middle|H-\epsilon_{\mathbf{k}j}\middle|\mathbf{k}j\right\rangle+\left\langle\mathbf{k}+\mathbf{q}j'\middle|H-\epsilon_{\mathbf{k}+\mathbf{q}j'}\middle|\sum_\alpha\ \delta^{\mathbf{q}\nu}\chi_\alpha^{\mathbf{k}}A_\alpha^{\mathbf{k}j}\right\rangle, \tag{17}$$

where $\delta^{\mathbf{q}\nu}\chi_\alpha^{\mathbf{k}}$ denotes the variation of the MT basis functions due to the phonon distortion of the $\mathbf{q}\nu$ mode. It is connected with the variation $\delta^+\chi_\alpha^{\mathbf{k}}/\delta R_\mu$ in the same way as for the induced potential, Eq. (2). Note that $\delta^{\mathbf{q}\nu}\chi_\alpha^{\mathbf{k}-\mathbf{q}}$ is a Bloch wave of the vector $\mathbf{k}$ since only this gives a nonzero contribution to the integral with $\psi_{\mathbf{k}j}$. The last two contributions in (17) represent the IBS corrections which are not vanished unless $\psi_{\mathbf{k}j},\psi_{\mathbf{k}+\mathbf{q}j'}$ are the exact solutions.

The key formula (17) can be understood very simply if we will interpret the electron-phonon matrix element as a splitting of the degenerate band $\epsilon_{\mathbf{k}j}=\epsilon_{\mathbf{k}+\mathbf{q}j'}=\epsilon_F$ due to the phonon distortion. As we discussed in I, the first-order correction to $\epsilon_{\mathbf{k}j}$ found as a change in the eigenvalue of the matrix problem contains both the expression of the standard perturbation theory as well as the incomplete-basis-set corrections [see formulas (9) and (12) in I]. It would be advantageous to use that formula because the eigenvalues of the matrix problem are variationally accurate for the whole range of parameters variation. It is a standard exercise to show that in the case of the degenerate band $\epsilon_{\mathbf{k}j}=\epsilon_{\mathbf{k}+\mathbf{q}j'}$ the development of the perturbation theory for the matrix eigenvalue problem will lead to the band splitting given by the formula (17).

The expression (17) is thus the linear-response analogy of evaluating the electron-phonon matrix elements via the splitting of the bands in the frozen-phonon method as done in Ref. 14. It is less sensitive to the errors in the wave functions introduced by the variational principle, has a correct long-wavelength behavior, and allows one to avoid the inclusion of d-f transitions in d-electron systems.

For the electron-phonon spectral distribution functions $\alpha^2F(\omega)$, we employ the expression[21] in terms of the phonon linewidths $\gamma_{\mathbf{q}\nu}$,

$$\alpha^2F(\omega)=\frac{1}{2\pi N(\epsilon_F)}\sum_{\mathbf{q}\nu}\frac{\gamma_{\mathbf{q}\nu}}{\omega_{\mathbf{q}\nu}}\delta(\omega-\omega_{\mathbf{q}\nu}), \tag{18}$$

where $N(\epsilon_F)$ is the electronic density of states per atom and per spin at the Fermi level. When the energy bands around

the Fermi level are linear in the range of phonon energies, the linewidth is given by the Fermi ''golden rule'' and is written as follows:

$$\gamma_{\mathbf{q}\nu}=2\pi\omega_{\mathbf{q}\nu}\sum_{\mathbf{k}jj'}|g^{\mathbf{q}\nu}_{\mathbf{k}+\mathbf{q}j',\mathbf{k}j}|^2\delta(\epsilon_{\mathbf{k}j}-\epsilon_F)\delta(\epsilon_{\mathbf{k}+\mathbf{q}j'}-\epsilon_F). \tag{19}$$

The spectral distribution function (18) and its first reciprocal moment λ are usually used to describe such important manifestation of the EPI as superconductivity and some normal-state properties. One such property is an enhancement of the electronic mass for the electron at the Fermi energy when its velocity $v_{\mathbf{k}}$ is reduced by the factor $1+\lambda_{\mathbf{k}}$ due to the interaction with phonons. The value of $\lambda_{\mathbf{k}}$ is given by the reciprocal moment of the so-called **k**-dependent electron-phonon spectral function $\alpha^2_{\mathbf{k}}F(\omega)$.This renormalization is observed in the de Haas–van Alphen and cyclotron-resonance experiments. As a consequence, the low-temperature electronic specific heat is also renormalized. For the latter effect it is sufficient to know only the Fermi-surface averaged value of $\lambda_{\mathbf{k}}$, i.e., λ.

A full description of the superconducting state can be obtained by solving the Eliashberg gap equations which relate the energy-gap function and the renormalization parameter for superconducting state to the electron-phonon and the electron-electron interactions in the normal state.[22] The electron-phonon-coupling function is given by $\alpha^2F(\omega)$. The Coulomb interaction is usually represented by some constant μ^*. A detailed nature of the effective Coulomb repulsion is not very well known. Fortunately, various definitions for μ^* have only a weak influence on the solution of the gap equations and its values can, e.g., be found by adjusting the calculated transition temperatures to the experimental ones.

Electron-phonon scattering has a dominant contribution to the electrical resistivity for reasonably pure metals except for the very low-temperature region where the impurity and electron-electron scattering are important. The influence of the EPI on the transport properties are described in terms of the transport spectral function[24] $\alpha^2_{\mathrm{tr}}F(\omega)=\alpha^2_{\mathrm{out}}F(\omega)-\alpha^2_{\mathrm{in}}F(\omega)$, where

$$\alpha^2_{\mathrm{out(in)}}F(\omega)=\frac{1}{N(\epsilon_F)\langle v_x^2\rangle}\sum_{\nu}\sum_{\mathbf{k}j\mathbf{k}'j'}|g^{\mathbf{k}'-\mathbf{k}\nu}_{\mathbf{k}'j',\mathbf{k}j}|^2 v_x(\mathbf{k})v_x(\mathbf{k}^{(')}) \times\delta(\epsilon_{\mathbf{k}j}-\epsilon_F)\delta(\epsilon_{\mathbf{k}'j'}-\epsilon_F)\delta(\omega-\omega_{\mathbf{k}'-\mathbf{k}\nu}). \tag{20}$$

Here $\langle v_x^2\rangle$ is the average square of the x component of the Fermi velocity. In the lowest-order variational approximation (LOVA) for the solution of the Boltzmann equation the expressions for electrical and thermal resistivities are

$$\rho(T)=\frac{\pi\Omega_{\mathrm{cell}}k_BT}{N(\epsilon_F)\langle v_x^2\rangle}\int_0^\infty\frac{d\omega}{\omega}\frac{x^2}{\sinh^2 x}\alpha^2_{\mathrm{tr}}F(\omega), \tag{21}$$

$$w(T)=\frac{6\Omega_{\mathrm{cell}}}{\pi k_BN(\epsilon_F)\langle v_x^2\rangle}\int_0^\infty\frac{d\omega}{\omega}\frac{x^2}{\sinh^2 x} \times\left[\alpha^2_{\mathrm{tr}}F(\omega)+\frac{4x^2}{\pi^2}\alpha^2_{\mathrm{out}}F(\omega)+\frac{2x^2}{\pi^2}\alpha^2_{\mathrm{in}}F(\omega)\right], \tag{22}$$

with $x=\omega/2k_BT$. The LOVA results (20), (22) give the upper bound to the resistivities and allow us to test the calculated $\alpha^2_{\mathrm{tr}}F(\omega)$.

III. RESULTS

A. Technicalities

Our calculations of phonon dispersions and electron-phonon interactions for the elemental metals such as fcc Al, Cu, Pb, Pd, and bcc Mo, Nb, Ta, V are performed in the framework of the linear-response LMTO method.[18] The details of the calculations are the following: We find the dynamical matrix and the phonon linewidths for these materials as a function of wave vector for a set of irreducible **q** points at the (8,8,8) reciprocal lattice grid [29 points per 1/48th part of the Brillouin zone (BZ)]. The (I,J,K) reciprocal lattice (or Monkhorst-Pack[25]) grid is defined in a usual manner: $\mathbf{q}_{ijk}=(i/I)\mathbf{G}_1+(j/J)\mathbf{G}_2+(k/K)\mathbf{G}_3$, where $\mathbf{G}_1$, $\mathbf{G}_2$, $\mathbf{G}_3$ are the primitive translations in the reciprocal space. The self-consistent calculations performed for every wave vector involve the following parameters: We use $3\kappa-spd-$ LMTO basis set (27 orbitals) with the one-center expansions performed inside the MT spheres up to $l_{\max}=6$. In the interstitial region the basis functions are expanded in plane waves up to the cutoff approximately corresponding to 70, 140, and 200 plane waves per s, p, and d orbitals, respectively. All semicore states lying higher than -4 Ry are treated as valence states in separate energy windows. The induced charge densities and the screened potentials are represented inside the MT spheres by spherical harmonics up to $l_{\max}=6$ and in the interstitial region by plane waves with the cutoff corresponding to the (16,16,16) fast-Fourier-transform grid in the unit cell of direct space.

The **k**-space integration needed for constructing the induced charge density and the dynamical matrix is performed over the (16,16,16) grid (145 points per 1/48th part of the BZ), which is twice denser than the grid of the phonon wave vectors **q**. We use the improved tetrahedron method of Ref. 26. However, the integration weights for the **k** points at this (16,16,16) grid have been found to take precisely into account the effects arising from the Fermi surface and the energy bands. This is done with help of the energies $\epsilon_{\mathbf{k}j}$ generated by the original full-potential LMTO method at the (32,32,32) grid (897 points per 1/48 BZ). The procedure is explained in paper I (Ref. 18) in detail and allows us to obtain more convergent results with respect to the number of **k** points.

The **k**-space integration for the phonon linewidths $\gamma_{\mathbf{q}\nu}$ is very slowly convergent because it involves two δ functions according to Eq. (19). It is performed with the help of the (32,32,32) grid in the BZ by means of the tetrahedron method of Ref. 27. The largest numerical error of $\alpha^2F(\omega)$ comes from the integration over **q** in the expression (18). Its magnitude, we estimated by performing the integration over

TABLE I. Comparison between calculated and experimental (Ref. 31) phonon frequencies (THz) at the high-symmetry points X, L for the fcc metals Al, Pb, Cu, Pd, and at the points H, N for the bcc metals V, Nb, Ta, Mo. Also listed are the theoretical-to-experimental volume ratios V/V_0 used in the calculations.

fcc‖bcc		Al	Pb	V	Nb	Ta	Mo	Cu	Pd
$X_L\|\|H_{LT}$	theory	9.51	1.80	8.03	6.43	5.13	5.71	7.69	7.17
	exp.	9.69	1.86		6.49	5.03	5.52	7.25	6.72
$X_T\|\|N_L$	theory	5.83	1.06	7.22	5.52	4.54	7.99	5.36	5.01
	exp.	5.78	0.89		5.66	4.35	8.14	5.13	4.64
$L_L\|\|N_{T_1}$	theory	9.84	2.18	4.76	3.94	2.65	5.74	7.77	7.39
	exp.	9.69	2.18		3.93	2.63	5.73	7.30	7.02
$L_T\|\|N_{T_2}$	theory	4.33	0.92	6.17	4.80	4.18	4.69	3.64	3.60
	exp.	4.19	0.89		5.07	4.35	4.56	3.42	3.34
V/V_0		0.955	1.002	0.990	0.972	0.974	0.971	0.985	0.975

merely the band-structure factor [which is $\gamma_{\mathbf{q}\nu}$ approximated by $\Sigma_{\mathbf{k}jj'}\delta(\epsilon_{\mathbf{k}j}-\epsilon_F)\delta(\epsilon_{\mathbf{k}+\mathbf{q}j'}-\epsilon_F)$] using, respectively, (8,8,8) and (32,32,32) grids and found to be not larger than 7% in all cases.

A few words should be said about the lattice parameters used in the calculations. It is known that the equilibrium cell volume V found theoretically by the corresponding LDA-based total-energy calculation is frequently obtained slightly lower than the experimental volume V_0. This usually leads to the calculated at V_0 phonon frequencies which are softer comparing to the experimental ones. Often, a better agreement with the experiment can be obtained by performing the linear-response calculations at the theoretical volume. This is, in principle, a justified procedure from theoretical point of view. Unfortunately, the prescription does not work when calculating the phonon linewidths and $\alpha^2_{\rm tr}F(\omega)$: the results of calculated electrical and thermal resistivities agree less well with the experiment. The reason for this discrepancy is connected with the sensitivity of these quantities to the shape of the Fermi surface. It turns out that the use of the Fermi surfaces calculated at the experimental lattice constants considerably improves the results. We can thus use theoretical volumes in the linear-response calculations of phonon dispersions and the electron-phonon matrix elements. To find the phonon linewidths and $\alpha^2_{\rm tr}F(\omega)$ we can use, on the other hand, the energy bands entered (19) which are generated at the experimental lattice constants. We understand that it is not a well justified procedure to use different lattice parameters in one calculation, but it somewhat helps to minimize the errors connected with the LDA by simple means. The actual volume ratios V/V_0 used in our calculations to find the changes in the one-electron potentials are listed in Table I.

Another comment concerns the choice of the exchange-correlation potential. The general strategy employed by us is to use the exchange-correlation formula which gives the best prediction of the cell volumes. The von Barth–Hedin-like formula after Ref. 28 is employed for all the metals except Cu and V. For the $3d$ metals we have found that this formula gives the theoretical volumes which are too small ($V/V_0 \sim 0.9$). For Cu and V the Ceperley-Alder form[29] of the exchange-correlation potential parametrized after Ref. 30 is used which gives the ratios V/V_0 being much closer to unity (see Table I).

Finally note that in Ref. 20 we have used a different method for treating the full-potential terms in the calculation which was based on the atomic cells and the one-center spherical-harmonic expansions.[23] This method is not directly applicable to calculate phonon dispersions for materials with open structures such as, e.g., the diamond structure and requires the replacement of empty sites of the lattice by empty spheres. This complicates the evaluation of the dynamical matrix. In I we have employed another approach based on the plane-wave expansions for the LMTO's in the interstitial region and have applied the method to calculate the phonon spectra in Si and NbC. While the materials considered in this work have close-packed bcc or fcc structures we also apply this method which is more general for practical use. Some of the results for Al, Nb, and Mo previously published[20] do not noticeably differ from those presented below in this paper.

B. Lattice-dynamical properties

In Table I we report the values of the calculated phonon frequencies at the high-symmetry points X and L for the fcc metals Al, Cu, Pb, and Pd as well as at the points H and N for the bcc metals Mo, Nb, Ta, and V. For the comparison, the experimental frequencies[31] are also listed in Table I along with the theoretical-to-experimental volume ratios which have been used in the calculations.

Our results for the phonon dispersions along several symmetry directions together with the corresponding densities of states for these materials are displayed in Figs. 1(a)–(h). The theoretical lines result from the interpolation between the calculated frequencies which are denoted by circles. Many neutron-diffraction measurements are available[31] for nearly all the metals considered here and these data are also shown in Fig. 1 by triangles. The only exception is V for which the dispersion relations cannot be studied with neutrons since V is an almost totally incoherent neutron scatterer. While some x-ray diffraction measurements exist in the literature[31] their accuracy seems to be less satisfactory than the corresponding

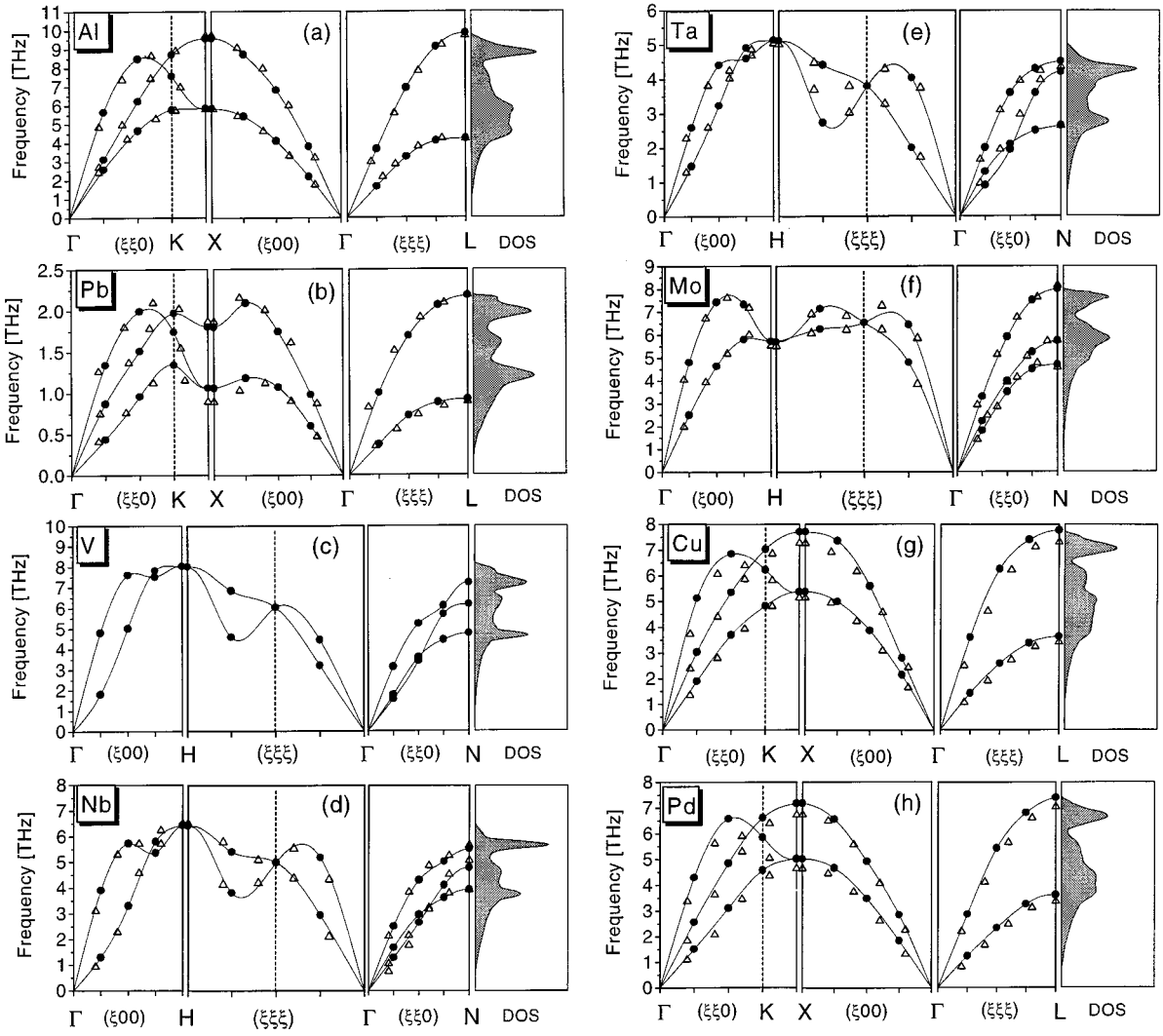

FIG. 1. (a)–(h) Calculated phonon-dispersion curves along several symmetry directions for the eight elemental metals considered in this work. The lines result from the interpolation between the theoretical points (circles). The results of available neutron-diffraction measurements (Ref. 31) are shown by triangles. Also plotted are the calculated densities of states (DOS).

neutron-scattering data for other materials and we do not show the experimental points for V.

From Fig. 1 we see that the agreement between theory and experiment is good. Most of the calculated frequencies agree within a few percent with those measured. This also follows from the numerical values listed in Table I. In particular, for Al [Fig. 1(a)] a very good agreement is found in all directions. As we have mentioned already, this calculation is performed at the theoretical volume ($V/V_0=0.955$). We have also checked the setup with the experimental volume and found a considerable softening (about 20%) of the transverse modes. This illustrates the importance of performing lattice-dynamical calculations at the theoretical volumes.

The most important consequence of our calculation for lead [Fig. 1(b)] is that the pronounced dip of both the longitudinal and transverse branches near the X point is well reproduced. We have also found a slight overestimate of the transverse phonon frequencies near this zone boundary which can be attributed neither to the discrepancy in the cell volume ($V/V_0=1.002$) nor to the neglection of the semicore states. (We have, in fact, included both $5d$ and $6d$ states in the main valence panel.) This kind of disagreement has also been recently reported in Ref. 32 using the linear-response pseudopotential technique. It is possibly connected with the use of the local density approximation or the lack of spin-orbit coupling effects in our calculation.

The most interesting cases are V, Nb, and Ta [Figs. 1(c), (d), (e), respectively]. The materials belong to group V of the Periodic Table and all of them show anomalous behavior of the phonon-dispersion curves. The presence of anomalies is, first of all, connected with the well-known dip of the longitudinal mode in the (00ξ) direction. The dip is correctly reproduced by our calculation. Other important features of our calculation are (i) the softening of the transverse mode along the (00ξ) direction at long wavelengths which is rather sharp in both V, Nb and is weaker in Ta as well as (ii) the crossover of two transverse branches in the $(\xi\xi0)$ direction. The latter is, in fact, predicted for Ta because the measured dispersions in this direction are absent for the T_1 branch except the zone-boundary point N.

The theoretical phonon dispersions for Mo also agree well with the experiment. The consequences of our calculations

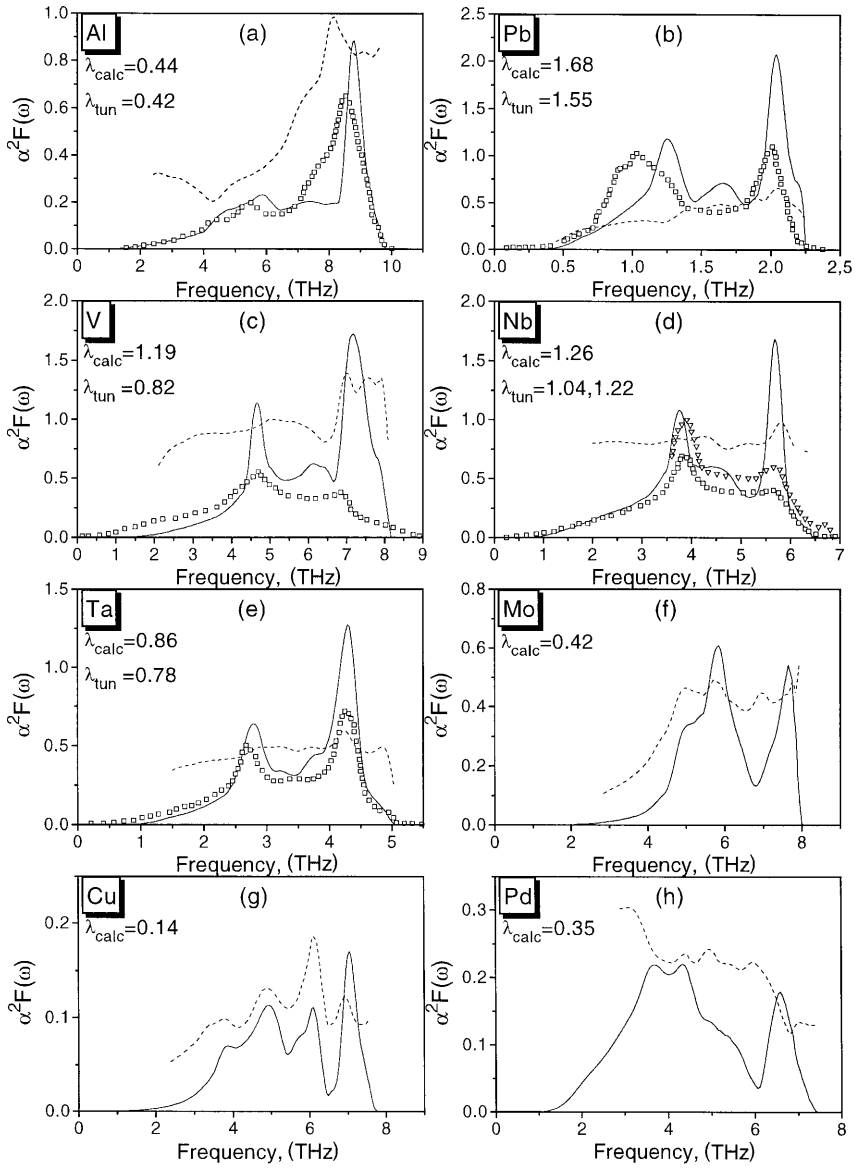

FIG. 2. (a)–(h) Calculated spectral functions $\alpha^2F(\omega)$ of the electron-phonon interaction (full lines) for the eight elemental metals considered in this work. The behavior of the electron-phonon prefactor $\alpha^2(\omega)$ [defined simply as the ratio $\alpha^2F(\omega)/F(\omega)$] is shown by dashed lines. Symbol plots present the results of available tunneling experiments (Refs. 3, 35, and 39).

here are the reproduced softening near the H point and the absence of the large dip along the $(\xi\xi\xi)$ direction near $\xi\sim 0.7$. The dip is presented in the dispersion curves of nearly all bcc metals except for Mo and Cr, and is certainly the feature of the behavior of the crystalline structure factor which enters the dynamical matrix as a sum over lattice vectors with the phase shift $\exp(i\mathbf{qt})$. Its absence indicates a considerable wave-vector dependence of the electron-phonon matrix elements which seems to be well reproduced by our method.

Finally, we compare the results of our calculations for Cu and Pd which are presented in Fig. 1(f) and Fig. 1(g). The dispersion relations for these materials do not show the anomalies and are smooth. A slight overestimation of the theoretical phonon frequencies is found for both these metals. The overestimation can likely be corrected by the use of the cell volumes in the calculation which would be slightly larger than those found within the LDA. However, such a procedure is not justified theoretically. We think that employing the gradient-corrected density functional[33] known to predict much better the equilibrium lattice parameter will allow us to improve these results.

C. Superconducting properties

We now discuss applications of our *ab initio* linear-response method to calculate the electron-phonon coupling and superconducting-state properties. First, we present our results for the spectral distribution functions and λ. Second, we describe our applications to solving the Eliashberg gap equations.

Calculated $\alpha^2F(\omega)$ for Al is shown in Fig. 2(a) (full line). The positions of the maxima here are conditioned by the form of the phonon density of states with the low-frequency phonon peak suppressed by the coupling function $\alpha^2(\omega)$ (dashed line). [The latter is defined simply as the ratio $\alpha^2F(\omega)$ to $F(\omega)$.] The broad phonon spectrum in Al is extended up to the maximal frequency $\omega_{\max}\approx 470$ K. The theoretical $\alpha^2F(\omega)$ in Fig. 2(a) is compared with the results of the tunneling measurements[3] (squares). We find a rather good agreement between the two curves. In fact, our $\alpha^2F(\omega)$ is also found to be practically identical to the empirical pseudopotential result of Ref. 34 based on the rigid-ion approximation. The latter is known to work well in simple metals. General agreement is found between our and

TABLE II. Comparison between the calculated electron-phonon coupling constants λ_{calc} and the values of λ_{tun} deduced from the tunneling experiments. Also listed are the values of λ_{s-h} extracted from the measured specific-heat coefficient γ with the use of our calculated density of states $N(\epsilon_F)$.

	Al	Pb	V	Nb	Ta	Mo	Cu	Pd
λ_{calc}	0.44	1.68	1.19	1.26	0.86	0.42	0.14	0.35
λ_{tun}	0.42[a]	1.55[a]	0.82[a]	1.04,[a] 1.22[b]	0.78[a]			
λ_{s-h}	0.43	1.64	1.00, 1.17	1.17	0.83	0.45		0.69
$N(\epsilon_F)$, $\frac{\text{states}}{\text{Ry}*\text{cell}}$	5.49	6.87	26.14	20.42	18.38	8.34	4.36	34.14
γ, $\frac{\text{mJ}}{\text{K}^2\text{mol}}$	1.36[c]	3.14[c]	9.04,[c] 9.82[d]	7.66[c]	5.84[c]	2.10[c]	0.69[c]	10.0[c]

[a]Reference 3.
[b]Reference 39.
[c]Reference 51.
[d]Reference 52.

the *ab initio* frozen-phonon results of Dacorogna *et al.*[12] for the dispersion of the phonon linewidths along the high-symmetry directions. The only exception is that, in the (00ξ) direction, our longitudinal branch of $\gamma_{\mathbf{q}\nu}$ exceeds theirs by a factor of 2. This is presumably connected with replacing the δ functions in (19) by Gaussians used in Ref. 12. However, the relative weight of our high γ values in the integrated quantities, such as $\alpha^2F(\omega)$ and λ, is found to be very small. Our value of λ is 0.44 which is very close to the value of $\lambda_{tun}=0.42$ extracted from the tunneling measurements.[3] The frozen-phonon[12] and linear-response calculations of Winter[15] gave, respectively, $\lambda=0.45$ and 0.38. The value of λ_{s-h} extracted from the electronic specific-heat coefficient γ and our calculated density of states $N(\epsilon_F)$ using the relation

$$1+\lambda_{s-h}=\frac{3\gamma}{2\pi^2 k_B N(\epsilon_F)}, \tag{23}$$

is 0.43 (see Table II). In order to check previous conclusions[15,40] about the inapplicability of the RMTA for sp metals, we also performed such a calculation and indeed found $\lambda_{RMTA}=0.14$.

Lead is a well-studied classical example of strong-coupled superconductor with $T_c=7.19$ K and its tunneling spectra have been studied a long time ago.[35] Obtained $\alpha^2F(\omega)$ using our linear-response method is presented in Fig. 2(b), where it is compared with the results of the measurements.[35] The two curves are similar. Our calculated $\lambda=1.68$ is found to be 8% larger than the tunneling value 1.55 and only 2% larger than the value 1.64 extracted from specific-heat data (see Table II). This disagreement is well within the accuracy of our calculation.

We now report our results for V, Nb, and Ta which are the best-studied elemental superconductors because of their relatively high-T_c values. Especially, for Nb which has the highest $T_c=9.25$ K among the elemental metals, there exist many experimental investigations of the tunneling spectra[36–39] and theoretical RMTA-based calculations.[40–42] Unfortunately, some of the results which have been reported in the literature are controversial. First, the RMTA calculations give the values of λ varying from 1.12 to 1.86. Second, the tunneling estimates of the coupling constant for Nb and V are difficult because of the oxidation of the surface layers. Having lower transition temperature, such oxides act on the tunneling spectra due to the proximity effect. The experimental λ in Nb varied in the past from the values[36] $0.58-0.68$ with negative or anomalously small μ^* to the value[37] 0.9. At present, a satisfactory explanation of the anomalous behavior of the thermally oxidized tunneling junctions in Nb appears to be possible which gives the values[38,39] of $\lambda_{tun}=0.92-1.22$.

In Figs. 2(c), (d), (e) we present our calculated $\alpha^2F(\omega)$ (full lines) for V, Nb, and Ta, respectively. They all have rather broad spectra extended up to $\omega_{max}\approx 370$ K, 310 K, and 240 K. The coupling function $\alpha^2(\omega)$ (dashed line) in these metals only slightly deviates from constant in a major part of the frequencies. The approximation $\alpha^2=\text{const}$ works very well in Nb and Ta. This qualitative result implies that the electron-phonon coupling can be factorized into electronic and phonon-dependent factors.[44,9]

In Fig. 2 the calculated spectral functions are compared with the results of the tunneling measurements (squares). As it can be seen for V [Fig. 2(c)], our $\alpha^2F(\omega)$ disagrees with the measured one[46] because of the appearance of the upper phonon peak not presented in the experiment. Even though the theoretical $\alpha^2F(\omega)$ should be broadened because the δ function in Eq. (18) ought to be a Lorentzian of half width $\gamma_{\mathbf{q}\nu}$, the electron-phonon coupling estimated by us $(\lambda=1.19)$ is $40-50\,\%$ stronger than the obtained $\lambda_{tun}=0.82$. The same situation is found for Nb. Our calculation here [Fig. 2(d)] also does not show the suppression of the longitudinal peak. The latter is absent in nearly all the experiments for this metal.[38] [A typical measured spectrum[3] is shown in Fig. 2(d) by squares]. As a result, the calculated $\lambda=1.26$ is 20% higher than $\lambda_{tun}=1.04$[3]. The discrepancy found by us has already been reported in the past RMTA-based calculations.[41,42] To check the consistency of our results with the earlier ones, we have performed our own RMTA calculations and obtained complete agreement between them. We thus conclude that the full inclusion of screening does not resolve the problem of the suppressed longitudinal peak.

Unfortunately, our comparison with the experiment is complicated by the proximity effect and the extraction of the tunneling densities of states depends on the way the measured data are processed. For example, in Nb the value of $\lambda_{tun}=1.22$ deduced from the tunneling experiments (which is only 3% lower than that found by us) has been reported in the literature.[39] The obtained $\alpha^2F(\omega)$ [denoted in Fig. 2(d) by triangles] is found much closer to our calculation.

A better understanding of the present situation can be achieved by comparing the theoretical and the experimental[47,3] tunneling spectra for Ta since its superconducting properties are close to those of V and Nb but this metal is much less reactive with oxygen. Such a comparison is given in Fig. 2(e). We find rather good agreement between both curves. In particular, the upper phonon peak is not suppressed in the measured $\alpha^2F(\omega)$and its amplitude is comparable with that calculated by us. As a result, the theoretical $\lambda=0.86$ agrees within 10% with the $\lambda_{tun}=0.78$.

In view of the data on Ta we cannot consider the discrepancy found for V and Nb as a drawback of either our linear-response method or the use of the local density approximation. Partially this conclusion is also verified by alternative estimates of the coupling constant based on the specific-heat data and the de Haas-van Alphen (dHvA) experiments, but it should be noted that both cyclotron masses and the specific-heat coefficient are also enhanced by the electron-electron interactions. Evaluation of the average coupling from the specific-heat measurements[51] yields an enhancement of 1.00 for V and 1.17 for Nb (see Table II). If one uses a more recent value[52] of γ for V rather than the one listed in Ref. 51 one obtains the enhancement $\lambda_{s-h}=1.17$, which nearly coincides in this metal with our $\lambda=1.19$. Comparison between the LDA band masses with those measured by the dHvA effect[48] yields the enhancement of 1.33 for Nb, which is close to the value 1.26 found in our calculation. Another important result is that the measured *variation* of the mass enhancement for the various cyclotron orbits in Nb agrees also well with our calculation. Namely, we have found a decomposition of λ by the Fermi-surface sheets: (i) octahedron, (ii) jungle gym, and (iii) ellipsoids, and have obtained the contributions $\lambda^{i}=1.44$, $\lambda^{ii}=1.37$, and $\lambda^{iii}=1.08$. They can be compared with the measured $\lambda^{i}_{dHvA}=1.71$,$\lambda^{ii}_{dHvA}=1.43$, and $\lambda^{iii}_{dHvA}=1.10$. (Note that the calculated within the RMTA anisotropy of the mass enhancement strongly disagrees with these data.[48]) Moreover, we have estimated the transport constants λ_{tr} for these metals both from the calculated and measured resistivity data. The values of λ_{tr} are usually believed to be close to the superconducting ones. (A complete report of our calculated transport properties will be given in the following subsection.) For V, the value of λ_{tr} found by us is 1.15 and, for Nb, $\lambda_{tr}=1.17$. The calculated electrical and thermal resistivities are also close to those measured. It therefore seems that our electron-phonon coupling is accurate (within the computational accuracy of order 10%) while the effect of the electron-electron interactions is small in these metals.

As the next two examples, we report the results of our applications for Mo and Cu. There are no tunneling data for these materials because of their low T_c and the weakness of phonon effects. The calculated spectral functions are presented in Figs. 2(f), (g). Both curves qualitatively agree with the corresponding phonon state densities shown for these metals in Figs. 1(f), (g), but a considerable frequency dependence of the electron-phonon prefactor $\alpha^2(\omega)$ (indicated by dashed lines) is also predicted. For Mo our linear-response calculations are found to be close to our RMTA calculations and to earlier ones.[49] The estimated average coupling here is 0.42 which can be compared with the value 0.45 deduced from the specific-heat measurements (see Table II). The calculated value of λ for Cu is 0.14. The specific-heat estimate here is less reliable possibly because of the smallness of λ and errors due to the experimental uncertainty in the value of γ. Quite likely, however, there are some errors in the DFT value of the density of states connected with the many-body effects since the copper valence shell $3d^{10}$ is close to the strongly correlated $3d^9$ configuration. It is known that within DFT the position of d band is higher than experimentally observed. The band which crosses the Fermi level is essentially s band but the effect of hybridization with the d band should lead to a lowering of the Fermi velocities. The latter effect is stronger if the d band is closer to the Fermi energy. To obtain $1+\lambda_{s-h}\sim 1.1$, one has to reduce our calculated $N(\epsilon_F)$ by approximately 20% which is a reasonable estimate for the expected influence of the Coulomb correlations. Concerning other estimates of λ based on the transport properties, our calculated $\lambda_{tr}=0.13$ while this value extracted from the measured resistivity data is 0.12 (see following subsection). Both values are in agreement with our superconducting λ.

As the last example, we consider Pd and discuss paramagnon effects. The superconductivity in Pd is absent because of the large spin fluctuations.[2] There was also a discussion in the literature[50] on the paramagnon contributions to the mass enhancement in Nb and V. The occurrence of paramagnons is connected with the fluctuations of the electron spins. Paramagnons usually counteract superconductivity since the latter has its origin in the formation of pairs with the opposite spins. To extract the paramagnon contribution, we can use our calculated values of λ together with the specific-heat[51,52] estimates λ_{s-h} after formula (23). The necessary data are listed in Table II. Comparing these results does not leave any place for $\lambda_{spin}=\lambda_{s-h}-\lambda$ in all the materials except in Pd which is a typical example for paramagnon effects. Here $\lambda_{s-h}=0.69$ and with the use of our calculated $\alpha^2F(\omega)$ [Fig. 2(h)], the average electron-phonon coupling is found to be equal to 0.35. This results in our value of $\lambda_{spin}=0.34$ for Pd which is close to its earlier estimate 0.31 based on the RMTA calculation.[43]

After comparing the calculated and experimental spectral functions, we present the results of our applications to solving the Eliashberg gap equation with our knowledge of $\alpha^2F(\omega)$. Having fixed the Coulomb pseudopotential μ^*, the superconducting state is now completely described by the strong-coupling theory of superconductivity.[22] According to the Allen-Dynes[45] modified McMillan[44] formula,

$$T_c^{\mathrm{McM}}=\frac{\omega_{\log}}{1.2}\exp\left(-\frac{1.04(1+\lambda)}{\lambda-\mu^*(1+0.62\lambda)}\right), \qquad (24)$$

the effect of the first reciprocal moment λ of $\alpha^2F(\omega)$ on T_c is most important. Unfortunately, the estimation of the coupling constant from T_c is difficult because of the un-

TABLE III. Calculated values of the Coulomb pseudopotential μ^* which provide the experimental values of T_c as the solutions of the Eliashberg equation with our knowledge of $\alpha^2F(\omega)$. Values T_c^{McM} were then found with our $\omega_{\log}$, λ, and μ^* in order to check the accuracy of the McMillan T_c expression. Also shown are the computed and the measured (Ref. 3) superconducting energy-gap parameters Δ_0.

	Al	Pb	V	Nb	Ta	Mo	Cu	Pd
μ^*	0.12	0.17	0.30	0.21	0.17	0.14	0.11	
T_c^{exp}, K	1.18	7.19	5.40	9.25	4.47	0.92	>0	
T_c^{McM}, K	1.22	6.81	6.68	10.5	5.11	0.67	>0	
$\omega_{\log}$, K	270	65	245	185	160	280	220	180
Δ_0^{calc}, meV	0.18	1.35	0.84	1.53	0.70	0.14		
Δ_0^{exp}, meV	0.18	1.33	0.81	1.56	0.71			

known value of μ^*. We use a standard Matsubara technique to solve numerically the Eliashberg equation for T_c and have found μ^* which gives the experimental value of T_c. The cutoff parameters ω_{cut} were taken to be equal to ten phonon-boundary frequencies $\omega_{\max}$. To treat the Coulomb pseudopotential in terms of the expression (24) when solving the Eliashberg equation, we have rescaled actually used parameters $\mu^*(\omega_{\mathrm{cut}})$ to $\mu^*=\mu^*(\omega_{\log})$ according to

$$\frac{1}{\mu^*}=\frac{1}{\mu^*(\omega_{\mathrm{cut}})}+ln\frac{\omega_{\mathrm{cut}}}{\omega_{\log}}. \tag{25}$$

Table III reports the obtained μ^* values. The main conclusion here is that the calculated μ^* varies between 0.11 and 0.17 which is close to the conventional value usually taken, ~ 0.13. The noticeable exceptions are only Nb and, especially, V for which too large μ^* have been found. Of course, this overestimation occurs over the conventional quantity 0.13 while the detailed theoretical data on the Coulomb pseudopotential are unknown. We think that the obtained quantities are still below the upper limit for the allowed μ^* values.

Also listed in Table III are the values of T_c^{McM} evaluated after (24) with our calculated $\omega_{\log}$, λ, and μ^*. As it can be seen, the exact solution of the Eliashberg equation gives T_c (chosen to be the experimental value) which slightly deviates from that estimated after the McMillan expression. The accuracy of the later is averagely about 15%.

To conclude that our spectral functions provide a proper description of superconductivity we have found the energy-gap parameters Δ_0. These results are shown in the last two rows of Table III. The available tunneling data for Al give Δ_0 coinciding with the theoretical value. Some overestimation of the coupling constant in comparing to the experimental one has taken place in Pb, while Δ_0 agrees very closely. Let us turn to the important case of transition metals V, Nb, and Ta. As we have discussed already, the main difficulties in the tunneling studies in V and Nb are connected with the oxidation of the surface layers and the tunneling estimations of the coupling constant in Nb varied considerably in the past. In contrast to it, the measured superconducting gap in Nb has approximately the same values in all the experiments and is equal to 1.56 meV.[3] This value perfectly agrees with that found by us which is equal to 1.53 meV. We have also found a good agreement in the energy gap for V which is within 4% of the experimental one. The discrepancy in the energy gap for Ta is again $1-2$ %. Because of the low transition temperature there is no tunneling data for Mo and we only give the theoretical value of Δ_0. We thus see that despite the discrepancy in evaluating the coupling constants, an extremely good agreement ($1-2$ %) is obtained for the predicted gap data. Such a coincidence is readily understood because the ratio $2\Delta_0/T_c$ is slowly varying for different superconductors. (It is 3.52 within the BCS theory.) Fixing the T_c to its experimental value makes the value of Δ_0 insensitive to the errors in $\alpha^2F(\omega)$ and λ.

To summarize, we have found that our results for the spectral functions and, in particular, for the coupling constants are realistic for the correct description of the superconducting properties. Especially, excellent agreement has been found between our calculated λ and the values extracted from specific-heat measurements. The values of λ deduced from the available tunneling experiments also agree within 10% with our calculations in all the materials except Nb and, especially, V. However, taking into account the past tendency to correct the tunneling spectra for Nb as well as our calculations for Ta, we do not consider these discrepancies as essential.

D. Transport properties

We now report the results of our applications for calculating the electron-phonon contribution to the electrical and thermal resistivities (conductivities). This field remains very important and interesting, first, because the easily measured transport properties and, especially, the electrical resistivities, provide valuable information on the electron-phonon-coupling strength and, second, no large-scale investigations of these properties by *ab initio* theoretical calculations appeared so far.

We calculate the electrical and thermal resistivity using the low-order variational approximation (LOVA) and our theoretical transport spectral functions found after Eq. (20). As follows from Eqs. (21) and (22) at high temperatures:

$$\rho=\frac{\pi\Omega_{\mathrm{cell}}k_BT}{N(\epsilon_F)\langle v_x^2\rangle}\lambda_{\mathrm{tr}}, \tag{26}$$

$$w=\frac{6\Omega_{\mathrm{cell}}}{\pi k_BN(\epsilon_F)\langle v_x^2\rangle}\lambda_{\mathrm{tr}}, \tag{27}$$

and important information is contained in the transport constant λ_{tr} defined by

$$\lambda_{\mathrm{tr}}=2\int_0^\infty\frac{d\omega}{\omega}\alpha_{\mathrm{tr}}^2F(\omega). \tag{28}$$

It is usually believed that the latter is close to the superconducting λ because the expressions for $\alpha_{\mathrm{tr}}^2F(\omega)$ and $\alpha^2F(\omega)$ are quite similar, except for the factor $[1-\mathbf{v}(\mathbf{k})\mathbf{v}(\mathbf{k}')/|\mathbf{v}(\mathbf{k})|^2]$, which preferentially weights the backscattering processes. However, there may exist a signifi-

TABLE IV. Comparison between calculated and empirical values of the transport constant λ_{tr}. The values of λ_{tr}^{exp} were deduced from the electrical-resistivity data (Ref. 55) with the help of our calculated bare plasma frequencies ω_p. Also listed are the average transport frequencies $\Theta_{tr}=\sqrt{\langle\omega^2\rangle_{tr}}$.

	Al	Pb	V	Nb	Ta	Mo	Cu	Pd
λ_{tr}^{calc}	0.37	1.19	1.15	1.17	0.83	0.35	0.13	0.43
λ_{tr}^{exp}	0.39	1.52	1.15	1.11	0.93	0.40	0.12	0.50
ω_p, eV	12.29	14.93	7.95	9.47	9.05	8.81	8.75	7.34
Θ_{tr}, K	330	75	260	200	170	290	230	190

cant difference between $\alpha_{tr}^2F(\omega)$ and $\alpha^2F(\omega)$ for the case of strongly nested Fermi surfaces[53] due to the contribution from the backscattering of electrons between the opposite sides of the nested Fermi surface.

Despite the complexity of the Fermi surfaces in the transition metals, we have obtained the transport functions $\alpha_{tr}^2F(\omega)$ quite close to the superconducting $\alpha^2F(\omega)$ which have been shown in Fig. 1. The latter is also true for the simple metals considered in this work. Unfortunately, we have not investigated an interesting question about the low-frequency behavior of the $\alpha_{tr}^2F(\omega)$ due to a relatively coarse grid of the phonon wave vectors used for integrating the Eq. (20). The values of λ_{tr} calculated from our transport functions are listed in Table IV. Comparison between λ_{tr} and superconducting constants calculated earlier (Table II) gives the difference between them within 20% in all the tested materials. This is in agreement with previous conclusions that $\lambda_{tr}\sim\lambda$ for transition metals.[54]

The results of our calculated electrical resistivity $\rho(T)$ and thermal conductivity $w^{-1}(T)$ are presented, respectively, in Fig. 3 and Fig. 4 (full lines), up to the temperatures 500 K. The symbols denote different measured points available from Refs. 55 and 56. (The residual values of the electrical resistivities are subtracted.) For the comparison with the experiment we are limited by the temperatures $T<2\Theta_{tr}$, where $\Theta_{tr}\sim\sqrt{\langle\omega^2\rangle_{tr}}$ is close to the average phonon energy. (We list our calculated values of Θ_{tr} in Table IV.)

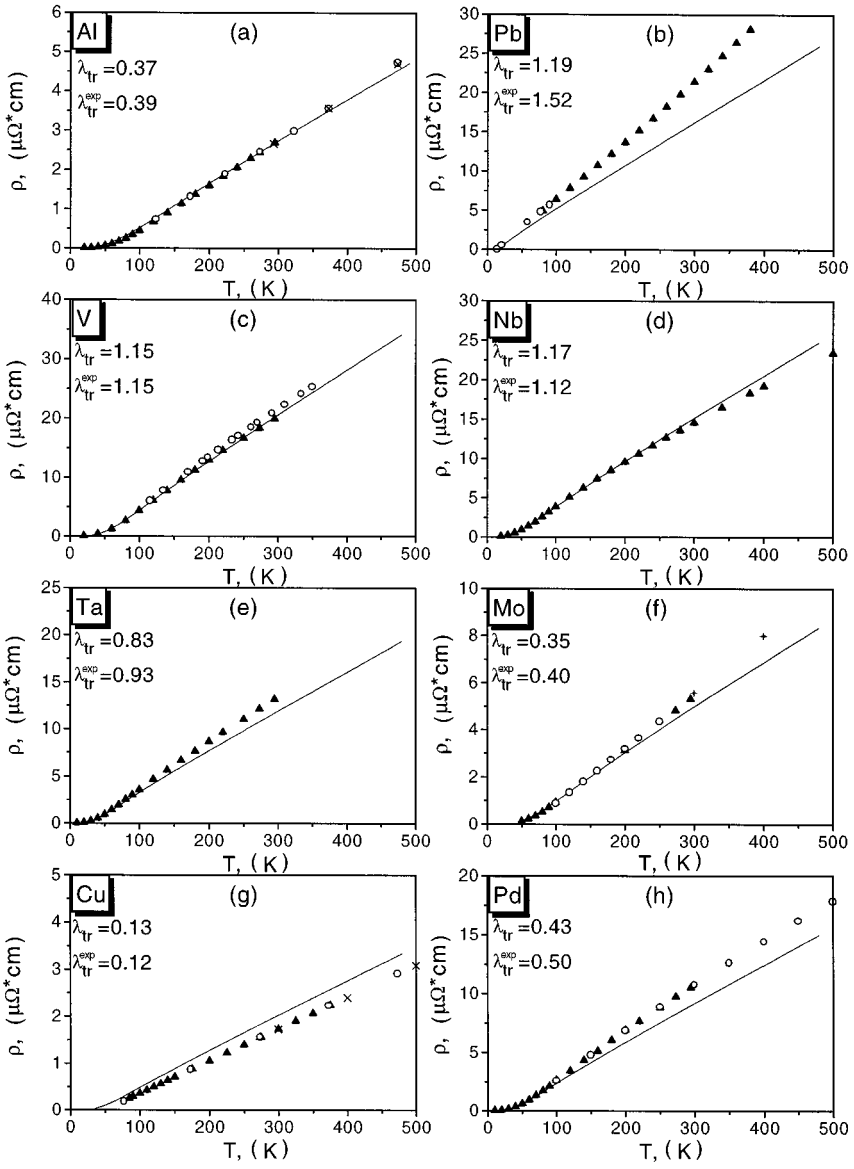

FIG. 3. (a)–(h) Calculated temperature dependence of the electrical resistivity, $\rho(T)$, as a lowest-order variational solution of the Boltzmann equation for the eight elemental metals considered in this work. Symbols show different experimental data available from Ref. 55.

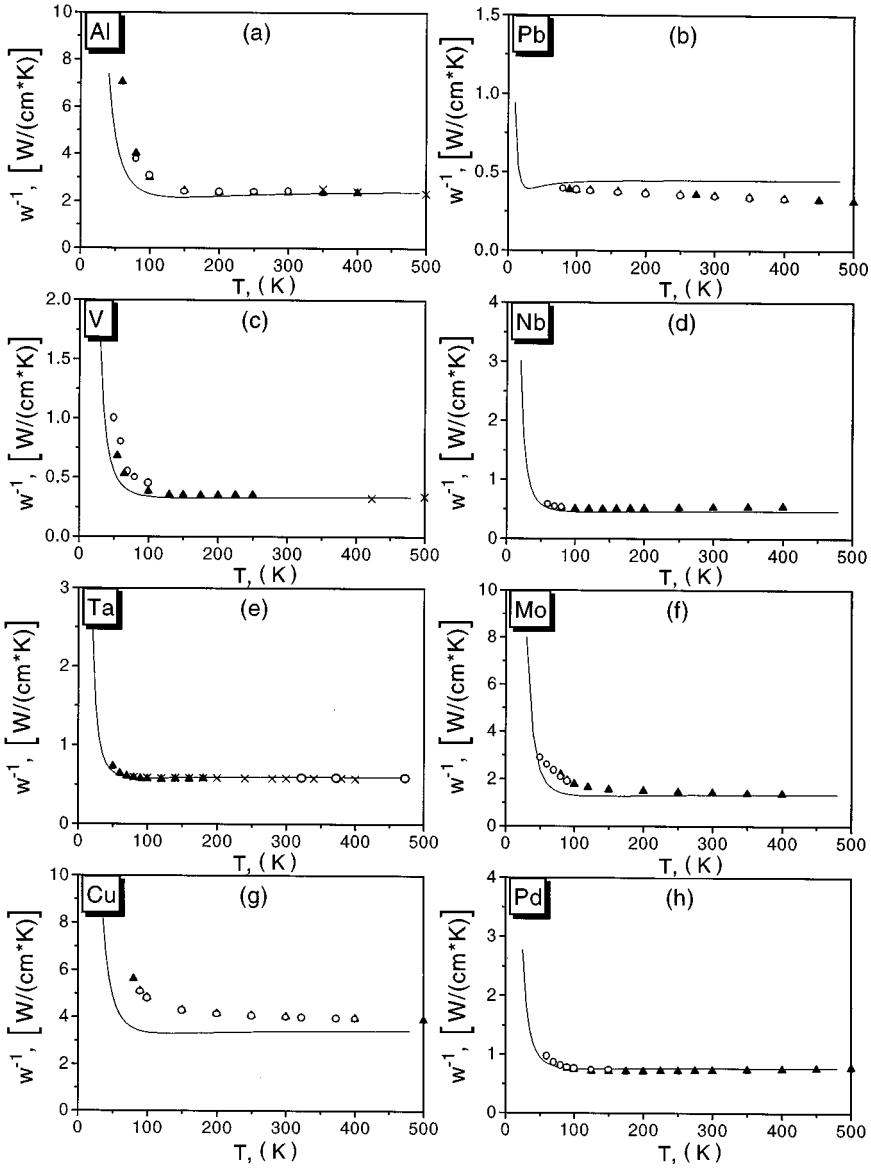

FIG. 4. (a)–(h) Calculated temperature dependence of the thermal conductivity, $w^{-1}(T)$, as a lowest-order variational solution of the Boltzmann equation for the eight elemental metals considered in this work. Symbols show different experimental data available from Ref. 56.

This is so because the description of the transport properties at high temperatures require us to take into account the anharmonicity effects and the Fermi-surface smearing. At low temperatures (usually when $T<\Theta_{\rm tr}/5$) the calculations will demand the inclusion of the N sheet[54] and the inelasticity corrections beyond LOVA.[54] Also, here a more careful integration over the Brillouin zone is necessary to produce a correct limit of $\alpha^2_{\rm tr}F(\omega)$ when $\omega\to 0$. Moreover, we cannot consider very low temperatures because of the effects of electron-electron scattering, size effects, impurity scattering, etc., which may give considerable contributions in addition to the electron-phonon scattering. The latter is basically responsible for the electrical resistivity of a metal at high temperatures in the absence of spin fluctuations. For the thermal conductivity, the lattice contribution to the heat current also exist and must be taken into account at the temperatures at least less than 100 K. From Table IV we see that, except lead, the values of $\Theta_{\rm tr}$ in all other materials are well above the low-temperature region and the comparison of our results with the measured ones must be relevant at the intermediate temperatures.

To compare the theoretical transport constants with the experiment, we fit the measured data[55] for $\rho(T)$ by a polynomial series

$$\rho(T)=\sum_{i=1}^{n} c_i T^{3-2i} \tag{29}$$

at the temperatures $\Theta_{\rm tr}/2<T<2\Theta_{\rm tr}$ with $n=2$. (The accuracy of the fit varies within 3% if n is increased.) The empirical values $\lambda_{\rm tr}^{\rm exp}$ were then found using the extracted coefficient c_1 as follows:

$$\lambda_{\rm tr}^{\rm exp}=\frac{c_1\omega_p^2}{8\pi^2 k_B}, \tag{30}$$

where ω_p is our calculated bare plasma frequency

$$\omega_p^2=\frac{8\pi N(\epsilon_F)\langle v_x^2\rangle}{\Omega_{\rm cell}}. \tag{31}$$

The obtained λ_{tr}^{exp} are shown in Table IV where they can be compared with our calculated λ_{tr}. Note that similar numerical estimates for λ_{tr}^{exp} can also be made by analyzing thermal conductivities because the measured Lorentz number approaches to the Sommerfeld value at the temperatures $T \geqslant \Theta_{tr}$.

For Al [Fig. 3(a)] we have found good agreement between the theoretical and the experimental[55] resistivities at the whole interval of the intermediate temperatures. The corresponding values of the transport constants are $\lambda_{tr}^{calc}=0.37$ and $\lambda_{tr}^{exp}=0.39$. The reduction of the coupling constant ($\lambda_{calc}=0.44$) to the transport one is less than 20%. There is also an agreement between the theoretical curve and the experimental points[56] for the thermal conductivity [Fig. 4(a)] above 150 K. The theory, however, underestimates $w^{-1}(T)$ at the lower temperatures. An obvious explanation here is the neglection of the lattice contribution to the thermal current. In fact, as can be seen from Fig. 4, such an underestimation at the low temperatures exist in all other materials considered in this work.

A comparison with the experiment is complicated for lead because of its low phonon energies ($\Theta_{tr}\sim 75$ K) and the importance of the anharmonic effects already at the low temperatures. The latter can possibly explain our discrepancy in the calculated electrical resistivity behavior shown in Fig. 3(b). The same disagreement exists in our results for the thermal conductivity, Fig. 4(b). Here, the discrepancy is minimal at the temperatures near 75 K and grows fastly as the temperature increases mainly because of the linear decay of the measured thermal conductivity. This obviously contradicts with the LOVA behavior of $w^{-1}(T)$ and is consistent with our assumption on the importance of the anharmonicity. Unlike in the other considered metals, the computed value 1.19 of the transport constant here is significantly smaller than the electron-phonon $\lambda=1.68$. This reduction could also point out the importance of the anisotropy in the electron-phonon scattering as well as the Fermi-surface effects which are not well reproduced by LOVA. In the absence of a calculation beyond LOVA it is difficult to determine the main source of errors.

Measured resistivity for Nb starts to saturate at high temperatures. In fact, this effect is evident [Fig. 3(d)] at the temperatures above $2\Theta_{tr}\sim 400$ K and it does not appear at the intermediate interval where the behavior of the resistivity only slightly deviates from the LOVA prediction. Comparing the calculated $\lambda_{tr}=1.17$ and the empirical values $\lambda_{tr}^{exp}=1.11$ gives the agreement about 5%. Like in Nb, there is a complete agreement between the theoretical and the experimental data for V [Fig. 3(c)] at the temperatures $\Theta_{tr}/5<T<2\Theta_{tr}$ (calculated $\Theta_{tr}\sim 260$ K). The theoretical $\lambda_{tr}=1.15$ coincides with the λ_{tr}^{exp} found empirically. The applicability of our method to the description of the transport properties for both V and Nb is also supported by comparing the thermal-conductivity data, Figs. 4(c) and 4(d).

Figure 3(e) and Fig. 4(e) present the results of our calculations in Ta. For $w^{-1}(T)$, an excellent correspondence of the theoretical prediction with observed behavior is obtained, but $\rho(T)$ is underestimated in our calculation within $10-12$ %. As a consequence, the evaluated $\lambda_{tr}^{exp}=0.93$ slightly exceeds the value 0.83 of the theoretical transport constant. The discrepancy is, in principle, within our computational errors. Note, however, that the experimental behavior[55] of $\rho(T)$ used in evaluating λ_{tr}^{exp} may depend on the sample purity and should be verified by several measurements. The disagreement can also be assigned to the influence of high-temperature effects in the vicinity of the upper limit ($2\Theta_{tr}\sim 340$ K) of the intermediate interval.

The results for Mo are given in Fig. 3(f) and Fig. 4(f). To avoid the influence of high-temperature effects we have dropped out the measured resistivity points at the temperatures above 300 K (the calculated $\Theta_{tr}\sim 290$ K). Fitting for $T<300$ K gives the result for the empirical transport constant $\lambda_{tr}^{exp}=0.40$ which is close to our prediction, $\lambda_{tr}^{calc}=0.35$. The agreement in the thermal-conductivity data is satisfactory for the whole intermediate interval.

The slope of the resistivity in Cu, Fig. 3(g), is also obtained quite accurate as in the other materials. The value of λ_{tr} is only slightly overestimated in the calculation. The discrepancy in the calculated thermal conductivity, Fig. 4(g), is larger and is about 20% at the room temperature. We cannot explain such disagreement by the renormalization due to the Coulomb correlations because, having been proportional to the ratio λ_{tr}/ω_p^2 both $\rho(T)$ and $w^{-1}(T)$ must be insensitive to this effect in the first order. The underestimation of the theoretical $w^{-1}(T)$ can point out the largeness of the lattice contribution to the thermal conductivity at the temperatures above 100 K. Unfortunately, there is a number of known difficulties to extract the latter values from the experiments.[57] From the low-temperature data analysis[57] one may conclude that the contribution to the thermal resistivity, w_{e-h}^{p}, from the process of a phonon decay by emitting electron-hole pairs is very small for Cu because of the apparently weak electron-phonon coupling ($\lambda\sim 0.12-0.14$). This supports our explanation for the obtained discrepancy.

Finally, the predicted transport properties of Pd are presented in Fig. 3(h) and Fig. 4(h). Like Cu, this metal has a $4d^{10}$ electronic configuration, but, in contrast to Cu, we have found a very good agreement between the calculated curve $w^{-1}(T)$ and its measured behavior. We can consequently judge that the thermal conductivity carried by phonons is small in this case which is consistent with the conclusion[57] that the contribution w_{e-h}^{p} is large for Pd. We have also found an underestimation of the electrical resistivity in the calculation. The agreement between λ_{tr} and λ_{tr}^{exp} (see Table IV) is about 15% which is, in principle, the upper limit of our computational uncertainty. Most likely, however, that the additional spin-fluctuation mechanism of the resistivity is also present in this metal.

In summary, the behavior of $\rho(T)$ and $w(T)$ is consistent with the results (26), (27) at the intermediate temperatures and there is no significant discrepancy between our calculations and the experimental points. More precisely, we have extracted the values of λ_{tr}^{exp} using the experimental data for $\rho(T)$ together with our band-structure value of ω_p and found the agreement between the experimental and the theoretical transport constants to be about 10% (in particular, lower than 5% for Al, Nb, Mo, and V). In fact, compared with the experiment is the ratio λ_{tr}/ω_p^2. Except possibly Cu and Pd, the DFT-based band-structure calculations assumed to provide the proper magnitude for the plasma frequency. So, we

drop the possibility of error cancellations and conclude that the theoretical λ_{tr} are in the real agreement with the experiment. A relatively high error level in Pb can be explained by the importance of the anharmonic effects. The large lattice contribution to the thermal conductivity could affect our comparison for Cu. In Pd, the additional mechanism of the resistivity can also take place. Nevertheless, taking into account the agreement in the other calculated properties, we think that our description of the electronic transport in the considered materials is quite satisfactory.

IV. CONCLUSION

We have presented *ab initio* linear-response calculations of the electron-phonon interaction in the transition metals Cu, Mo, Nb, Pd, Ta, V, and in the *sp* metals Al, Pb using the local density-functional method and the LMTO basis set. Our results for the lattice dynamical, superconducting, and transport properties in these materials agree well with the experiment. They can be summarized as follows: (i) we have obtained tunneling spectral functions $\alpha^2F(\omega)$ and their first reciprocal moments λ close to the measured ones; (ii) the correct values for the superconducting energy gap have been found using our calculated $\alpha^2F(\omega)$ and μ^* corresponding to the experimental T_c; (iii) the solution of the Eliashberg equation for T_c (or for μ^* if T_c is fixed) is well approximated by the conventional McMillan formula; (iv) the mass enhancement observed in the specific-heat measurements corresponds very well to our calculations and there is no paramagnon contribution in all the metals except Pd; (v) we have found the electrical and thermal resistivities in agreement with the measured data; (vi) we have also found them to be well described by the LOVA expressions; (vii) the theoretical transport constants agree with the values of λ_{tr}^{exp} within 10%. To summarize all of these results, we conclude that our method gives the description of the electron-phonon coupling with the accuracy of order 10%. We also conclude that the effect of renormalization of the energy bands due to electron-electron interactions is small (less than 20%, strictly speaking) in all considered materials. Some discrepancies between the theoretical and the tunneling values of λ in Nb and V can be assigned to the difficulty in processing the tunneling data. Nevertheless, it seems to us that more experimental and theoretical work is necessary to account for the large λ and μ^* in Nb and, especially, in V.

ACKNOWLEDGMENTS

The authors are indebted to O. K. Andersen, O. V. Dolgov, O. Jepsen, A. Liechtenstein, E. G. Maksimov, I. I. Mazin, and S. Shulga for many helpful discussions. One of us (D.Y.S.) was partially supported by Grant Nos. INTAS(93-2154), ISF(MF-8300), and RFFI.

[1] For a review, see, e.g., G. Grimvall, in *Electron-Phonon Interactions in Metals*, edited by E. P. Wohlfarth (North-Holland, Amsterdam, 1981).

[2] For a review, see, e.g., G. Gladstone, M. A. Jensen, and J. R. Schrieffer, in *Superconductivity*, edited by R. D. Parks (Dekker, New York, 1969), Vol. 2.

[3] For a review, see, e.g., E. L. Wolf, in *Principles of Electronic Tunneling Spectroscopy* (Oxford University Press, New York, 1985).

[4] P. Hohenberg and W. Kohn, Phys. Rev. **136**, B864 (1964).

[5] W. Kohn and L. J. Sham, Phys. Rev. **140**, A1133 (1965).

[6] For a review, see, e.g., *Theory of the Inhomogeneous Electron Gas*, edited by S. Lundqvist and S. H. March (Plenum, New York, 1983).

[7] For a review, see, e.g., B. M. Klein and W. Pickett, in *Superconductivity in d- and f-Band Metals*, edited by W. Buckel and W. Weber (Kernforschungszentrum, Karlsruhe, 1982), p. 477.

[8] L. J. Sham and J. M. Ziman, in *Solid State Physics*, edited by H. Ehrenreich and D. Turnbull (Academic, New York, 1963), Vol. 15, p. 221.

[9] G. D. Gaspary and B. L. Gyorfy, Phys. Rev. Lett. **28**, 801 (1972).

[10] W. H. Butler, in *Physics of Transition Metals, 1980*, edited by P. Rhodes, IOP Conf. Proc. No. 55 (Institute of Physics and Physical Society, London, 1981), p. 505.

[11] For a review of supercell and perturbative approaches, see, e.g., *Ab Initio Calculations of Phonon Spectra*, edited by J. T. Devreese, V. E. Van Doren, and P. E. Van Camp (Plenum, New York, 1983).

[12] M. M. Dacorogna, M. L. Cohen, and P. K. Lam, Phys. Rev. Lett. **55**, 837 (1985).

[13] T. W. Barbee, A. Garcia, M. L. Cohen, and J. L. Martins, Phys. Rev. Lett. **62**, 1150 (1989); R. E. Cohen, W. H. Pickett, and H. Krakauer, *ibid*. **64**, 2575 (1990).

[14] A. I. Liechtenstein, I. I. Mazin, C. O. Rodriguez, O. Jepsen, O. K. Andersen, and M. Methfessel, Phys. Rev. B **44**, 5388 (1991).

[15] H. Winter, J. Phys. F **11**, 2283 (1981).

[16] S. Baroni, P. Giannozzi, and A. Testa, Phys. Rev. Lett. **58**, 1861 (1987); N. E. Zein, Fiz. Tverd. Tela (Leningrad) **26**, 3028 (1984) [Sov. Phys. Solid State **26**, 1825 (1984)].

[17] R. M. Sternheimer, Phys. Rev. **96**, 951 (1954); **107**, 1565 (1957); **115**, 1198 (1959).

[18] S. Y. Savrasov and O. K. Andersen, preceding paper, Phys. Rev. B **54**, 16 470 (1996).

[19] O. K. Andersen, Phys. Rev. B **12**, 3060 (1975).

[20] S. Y. Savrasov, D. Y. Savrasov, and O. K. Andersen, Phys. Rev. Lett. **72**, 372 (1994).

[21] P. B. Allen, Phys. Rev. B **6**, 2577 (1972).

[22] G. M. Eliashberg, Zh. Éksp. Teor. Fiz. **38**, 966 (1960) [Sov. Phys. JETP **11**, 696 (1960)].

[23] S. Y. Savrasov and D. Y. Savrasov, Phys. Rev. B **46**, 12 181 (1992).

[24] P. B. Allen, Phys. Rev. B **31**, 305 (1971).

[25] H. J. Monkhorst and J. D. Pack, Phys. Rev. B **13**, 5188 (1976).

[26] P. Blöchl, O. Jepsen, and O. K. Andersen, Phys. Rev. B **49**, 16 223 (1994).

[27] P. B. Allen, Phys. Status Solidi B **120**, 529 (1983).

[28] U. von Barth and L. Hedin, J. Phys. C **5**, 1629 (1972); V. L. Moruzzi, J. F. Janak, and A. R. Williams, *Calculated Electronic Properties of Metals* (Pergamon, New York, 1978).

[29] D. M. Ceperley and B. J. Alder, Phys. Rev. Lett. **45**, 566 (1980).

[30] S. H. Vosko, L. Wilk, and M. Nusair, Can. J. Phys. **58**, 120 (1980).

[31] *Phonon States of Elements. Electron States and Fermi Surfaces of Alloys*, edited by K.-H. Hellwege and O. Madelung, Landolt-Börnstein, New Series, Group III, Vol. 13, Pt. a (Springer-Verlag, Berlin, 1981).

[32] S. de Gironcoli, Phys. Rev. B **51**, 6773 (1995).

[33] J. P. Perdew and Y. Wang, Phys. Rev. B **33**, 8800 (1986).

[34] H. K. Leung, J. P. Carbotte, D. W. Taylor, and C. R. Leavens, Can. J. Phys. **54**, 1585 (1976); see, also, *Principles of Electronic Tunneling Spectroscopy* (Ref. 3).

[35] See, e.g., W. L. McMillan and J. M. Rowell, in *Superconductivity*, edited by R. D. Parks (Dekker, New York, 1969), Vol. 1.

[36] J. Bostock, V. Diadiuk, W. N. Cheung, K. H. Lo, R. M. Rose, and M. L. A. MacVicar, Phys. Rev. Lett. **36**, 603 (1976); K. Gärtner and A. Hahn, Z. Naturforsch. Teil A **31**, 361 (1976).

[37] B. Robinson, T. H. Geballe, and J. M. Rowell, in *Superconductivity in d- and f-Band Metals*, edited by D. H. Douglas, AIP Conf. Proc. No. 4 (AIP, New York, 1974), p. 381.

[38] G. B. Arnold, J. Zasadzinski, and E. L. Wolf, Phys. Lett. **69A**, 136 (1978); E. L. Wolf, J. Zasadzinski, J. W. Osmun, and G. B. Arnold, J. Low Temp. Phys. **40**, 19 (1980).

[39] M. J. Bostock, M. L. A. MacVicar, G. B. Arnold, J. Zasadzinski, and E. L. Wolf, in *Proceedings of the Third International Conference on Superconductivity of d- and f-Band Metals*, edited by H. Suhl and M. B. Maple (Academic Press, New York, 1980), p. 153.

[40] D. A. Papaconstantopoulus, L. L. Boyer, B. M. Klein, A. R. Williams, V. L. Moruzzi, and J. F. Janak, Phys. Rev. B **15**, 4221 (1977).

[41] W. H. Butler, H. G. Smith, and N. Wakabayashi, Phys. Rev. Lett. **39**, 1004 (1977); W. H. Butler, F. J. Pinski, and P. B. Allen, Phys. Rev. B **19**, 3708 (1979).

[42] B. N. Harmon and S. K. Sinha, Phys. Rev. B **16**, 3919 (1977); D. Glötzel, D. Rainer, and H. R. Schober, Z. Phys. B **35**, 317 (1979); M. Peter, T. Jarlborg, M. Dacorogna, and E. Moser, in *Superconductivity in d- and f-Band Metals* (Ref. 7), p. 515.

[43] F. J. Pinski and W. H. Butler, Phys. Rev. B **19**, 6010 (1979).

[44] W. L. McMillan, Phys. Rev. **167**, 331 (1968).

[45] P. B. Allen and R. C. Dynes, Phys. Rev. B **12**, 905 (1975).

[46] J. Zasadzinski, D. M. Burnell, E. L. Wolf, and G. B. Arnold, Phys. Rev. B **25**, 1622 (1982).

[47] L. Y. Shen, Phys. Rev. Lett. **24**, 1104 (1970).

[48] G. W. Crabtree, D. H. Dye, D. P. Karim, D. D. Koelling, and J. B. Ketterson, Phys. Rev. Lett. **42**, 390 (1979).

[49] See *Principles of Electronic Tunneling Spectroscopy* (Ref. 3), p. 263, and references therein.

[50] H. Rietschel and H. Winter, Phys. Rev. Lett. **43**, 1256 (1979).

[51] K. A. Geschneidner, in *Solid State Physics: Advances in Research and Applications*, edited by H. Ehrenreich, F. Seitz, and D. Turnbull (Academic Press, New York, 1964), Vol. 16, p. 275.

[52] R. Radebaugh and P. H. Keesom, Phys. Rev. **149**, 217 (1966).

[53] V. H. Grespi and M. L. Cohen, Solid State Commun. **81**, 187 (1992).

[54] E. J. Pinski, P. B. Allen, and W. H. Butler, Phys. Rev. B **23**, 5080 (1981).

[55] *Metals: Electronic Transport Phenomena. Metalle: Elektronische Transport phänomene*, edited by K.-H. Hellwege and O. Madelung, Landolt-Börnstein, New Series, Group III, Vol. 15, Pt. a (Springer-Verlag, Berlin, 1982).

[56] *Metals: Electronic Transport Phenomena. Metalle: Elektronische Transportphänomene*, edited by K.-H. Hellwege and O. Madelung, Landolt-Börnstein, New Series, Group III, Vol. 15, Pt. c (Springer-Verlag, Berlin, 1982).

[57] W. H. Butler and R. K. Williams, Phys. Rev. B **18**, 6483 (1978).